Increase in internal quantum efficiency in small molecular oligothiophene: C_{60} mixed heterojunction solar cells by substrate heating

D. Wynands,[1,a)] M. Levichkova,[1] K. Leo,[1] C. Uhrich,[2] G. Schwartz,[2] D. Hildebrandt,[2] M. Pfeiffer,[2] and M. Riede[1]
[1]*Institut für Angewandte Photophysik, Technische Universität Dresden, 01062 Dresden, Germany*
[2]*Heliatek GmbH, 01139 Dresden, Germany*

(Received 9 May 2010; accepted 12 July 2010; published online 19 August 2010)

We present small molecule solar cells with α,ω-bis-(dicyanovinylene)-sexithiophene:C_{60} mixed heterojunctions, reaching power conversion efficiencies of $4.9 \pm 0.2\%$. We use substrate heating during deposition of the mixed layer to achieve an optimized morphology and show that this significantly improves the internal quantum efficiencies (IQEs) to values approaching 70%. By optical modeling, we evaluate the amount of loss due to absorption in inactive layers and show that IQE of the active layer itself is about 80%. © *2010 American Institute of Physics*. [doi:10.1063/1.3475766]

Organic solar cells offer the potential for a low-cost, easily processable, and flexible renewable energy source. Over the past decade mixed heterojunction (HJ) solar cells, where donor material and acceptor material are mixed in one layer, became the prevailing concept and efficiencies approaching 6% have been reported.[1,2] When a mixed HJ is employed, the optimization of the nanomorphology is very crucial. Depending on the scale of phase separation, donor and acceptor phase will interpenetrate each other on either small or large scales. A good interpenetration with small domain sizes, eventually below the exciton diffusion length, means that nearly all excitons can travel to a dissociating donor-acceptor (D-A) interface. However, a too small domain size is detrimental for charge transport because of discontinuous percolation pathways. The probability that a charge recombines with its opposite before reaching the electrode is then higher and consequently the charge collection efficiency decreases. Therefore, there is a tradeoff between efficient dissociation of excitons on one hand and loss-free charge carrier transport on the other hand, which makes control of the nanomorphology essential for reaching a high internal quantum efficiency (IQE) of the device.[3] Many studies have addressed the characterization and optimization of the morphology of polymer and small molecule mixed HJs.[4–8]

For the material system α,ω-bis-(dicyanovinylene)-sexithiophene (DCV6T):C_{60},we have already shown a significant improvement of the power conversion efficiency (PCE) to 3.8% by using elevated substrate temperatures (T_{sub}) to control the morphology.[9] Here, we present solar cells using DCV6T in an subsequently optically optimized layer structure, and discuss the role of IQE in such devices. The chemical structure of DCV6T-Bu(1,2,5,6) (DCV6T) which is introduced here is similar to the previously presented DCV6T-Et(2,2,5,5),[9] except for length and position of the alkyl side chains. It has a maximum absorption coefficient of $(3.2 \pm 0.3) \times 10^5$ cm^{-1} at 594 nm and the optical gap is 1.70 ± 0.02 eV (Fig. 1).

Devices were fabricated on indium tin oxide (ITO) covered glass substrates (Thin Film Devices Inc.). To place the active layers in the maximum of the optical field distribution transparent wide gap materials *N*,*N*′-diphenyl-*N*,*N*′-bis(4′-(*N*,*N*-bis(naphth-1-yl)-amino)-biphenyl-4-yl)-benzidine (Di-NPD, Sensient) and 9,9-bis[4-(*N*,*N*-bis-biphenyl-4-yl-amino)phenyl]-9H-fluorene (BPAPF, Lumtec) were used as hole transport layers. The device structure of the investigated samples A, B, and C is (thickness given in nanometer): ITO/n-C_{60}(5)/C_{60}(15)/DCV6T:C_{60} (x, T_{sub})/BPAPF (5)/p-BPAPF (10)/p-Di-NPD (30)/NDP9 (1)/Al (100). Device A was produced without substrate heating (T_{sub}=30 °C), whereas devices B and C were heated to a substrate temperature of approximately 90 °C during the deposition of the mixed layer. The mixing ratio of DCV6T:C_{60} is 2:1 by volume. The mixed layer thickness of devices A to C is x_A =30 nm, x_B=30 nm, and x_C=40 nm, respectively. For doping of C_{60}, the n-dopant NDN1 from Novaled AG (Dresden, Germany) was used with a ratio of 3 wt % (weight percent). BPAPF and Di-NPD were doped with the p-dopant NDP9 from the same company and a ratio of 10 wt % and 5 wt %, respectively. NDN1 and NDP9 are chosen for stability reasons, similar electrical properties can be achieved with dopants described, e.g., in Ref. 10. Current-voltage (J-V) characteristics were recorded with a source measure unit 236 SMU (Keithley) under a sun simulator SC-1200 (Steuerna-

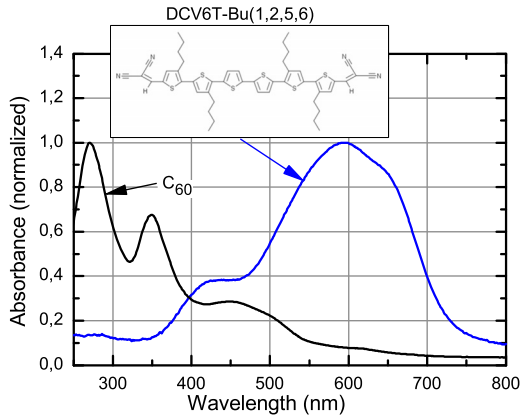

FIG. 1. (Color online) Absorbance of C_{60} and the donor material DCV6T-Bu(1,2,5,6). The chemical structure of DCV6T-Bu(1,2,5,6) is depicted in the inset.

[a)]Electronic mail: david.wynands@iapp.de.

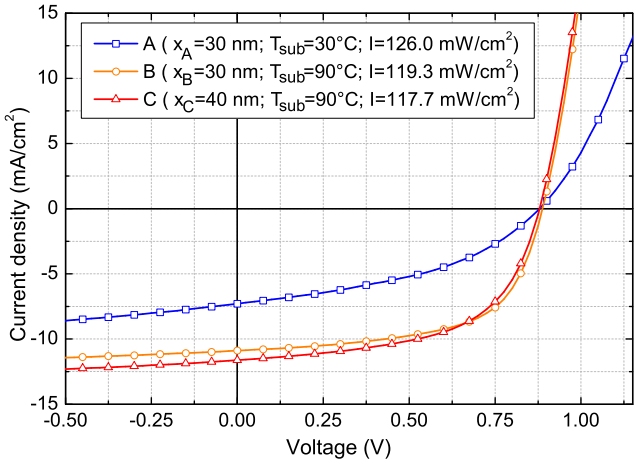

FIG. 2. (Color online) Current-voltage characteristics of devices A, B, and C. For performance parameters see Table I.

gel). The intensity determined by an outdoor reference cell (Fraunhofer Institute for Solar Energy Systems) was subsequently corrected for the spectral mismatch. The active area of the solar cells is 6.4 ± 0.2 mm^2. For the measurement of the external quantum efficiency (EQE), a home made setup based on a xenon arc lamp, a monochromator (Cornerstone 260), and a lock-in amplifier (Signal Recovery SR 7265) was used. Absorption spectra of the solar cells were measured in reflection geometry in a two-beam spectrometer UV 3100 (Shimadzu Corporation) using a pinhole mask with an area of 4.5 mm^2. To separate the absorption of active absorber layers from absorption within transport layers and metal contact, we model the device optically by using transfer-matrix-formalism.[11]

In Fig. 2 J-V characteristics of devices A to C are shown. The characteristic parameters of these devices are summarized in Table I. Apparently, devices B and C exhibit increased short circuit current (j_{sc}) and fill factor (FF) compared to device A. This is attributed to the change in mixed layer morphology induced by the applied substrate heating. As discussed previously, we expect a stronger phase separation when the substrate is heated during the deposition providing better charge transport within the percolation pathways of the mixed layer.[9] Consequently, devices B and C are both reaching increased PCEs of $4.9 \pm 0.2\%$. See Ref. 12 for additional verification of the PCE in an outdoor measurement. The advantage of the improved phase separation is also illustrated in the development of the IQE. Here, the IQE spectra given as follows:

$$\mathrm{IQE} = \eta_{\mathrm{ed}} \cdot \eta_{\mathrm{ct}} \cdot \eta_{\mathrm{cc}} = \frac{\mathrm{EQE}}{\eta_{\mathrm{a}}}, \tag{1}$$

are calculated from the measured absorption (η_a) and EQE spectra. This allows to discuss the role of the combined internal efficiencies of exciton diffusion to an interface (η_{ed}), exciton dissociation into charge carriers (η_{ct}), and charge collection (η_{cc}) separated from the probability of absorption. In Fig. 3 the respective spectra of absorption, EQE, and IQE are presented. Absorption spectra of devices A and B are nearly equal while device C shows increased absorption according to its larger layer thickness. The EQE spectra of devices A and B significantly differ and show a substantial increase for the heated device B. Device C exhibits the highest EQE reaching values of 61% in the maximum at 580 nm. The resulting IQE spectra clearly demonstrate the positive effect of substrate heating. Devices B and C are characterized by high IQE values above 70% from 550 to 620 nm while IQE of the nonheated device is significantly lower. This effect can mainly be attributed to the increase in η_{cc} due to improved phase separation. Despite the variation in mixed

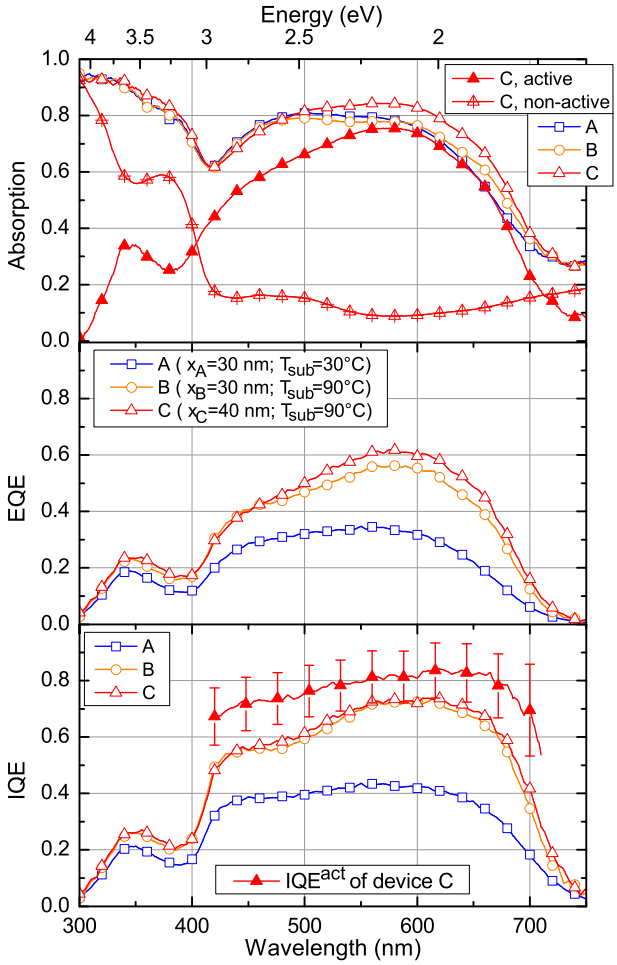

FIG. 3. (Color online) Absorption, EQE, and IQE of devices A, B, and C. For device C the simulated absorption of active (15 nm C_{60}+40 nm DCV6T:C_{60}) and nonactive (all other) layers as well as the corresponding IQE of the active layer are plotted.

TABLE I. Performance parameters of devices A, B, and C.

Device	V_{oc} (V)	j_{sc} (mA cm^{-2})	FF	I (mW cm^{-2})	η_{PCE} (%)
A	0.88	7.3	0.422	126.0	2.1 ± 0.1
B	0.89	10.9	0.607	119.3	4.9 ± 0.2
C	0.88	11.6	0.570	117.7	4.9 ± 0.2

layer thickness, all heated devices exhibit nearly equal IQE spectra. Furthermore they show a remarkably strong dependency on wavelength. See Ref. 12 for an additional device with $x_E=20$ nm, showing the same behavior. We can discuss these characteristics properly by using optically modeled absorption to subtract the absorption of nonactive layers from the measured total absorption. The corresponding spectra for device C are presented in Fig. 3. Active layers are the intrinsic C_{60} layer (15 nm) and the mixed layer ($x_C=40$ nm). All other layers are considered as nonactive. Below 400 nm, absorption of nonactive layers dominates the device total absorption. This is mainly caused by absorption of the transport layers. Accordingly, the IQE is significantly decreased in this region and shows a strong dependency on wavelength by following the development of active absorption versus total absorption. Above 400 nm, absorption in nonactive layers is only between 10% and 20% and mainly caused by the metal layer. With the given absorption of active layers (η_a^{act}), we can further establish a modified IQE^{act}

$$IQE^{act} = \frac{EQE}{\eta_a^{act}}, \tag{2}$$

which is only dependent on processes within the active layers and has no more influence of parasitic absorption. IQE^{act} of device C is presented in Fig. 3 (plotted for wavelength range where η_a^{act} is the dominating part). Apparently, high IQE^{act} values up to 83% are achieved at a wavelength of 610 nm, decreasing to 67% at a wavelength of 420 nm. The reason for this decline can be found in the different exciton diffusion efficiency (η_{ed}) for C_{60} and DCV6T excitons. In particular, excitons created in the intrinsic C_{60} layer which is adjacent to the mixed layer have a lower probability to reach a D-A interface since they might also migrate into the n-doped C_{60} layer and recombine there. Therefore, IQE^{act} is lower in the wavelength range dominated by C_{60} absorption. Besides this effect, the mixed DCV6T:C_{60} layer itself exhibits a very high IQE^{act}, which means that the mixed layer morphology in the heated device is considerably optimized and consequently the thickness dependence of η_{cc} is rather small upon the investigated interval of 20 to 40 nm.

The total amount of losses can be evaluated using the presented spectra. Assuming a sun illumination as defined by the spectrum AM1.5 G (standard: ASTM G 173), we calculate the absorbed photon flux in the devices to determine a maximum current j^{max} which is associated to 100% effective conversion of those absorbed photons into current. For this, a wavelength range of 300–750 nm is used. Device A, B, and C exhibit $j^{max}_{device,A}=15.4$ mA cm^{-2}, $j^{max}_{device,B}=15.6$ mA cm^{-2}, and $j^{max}_{device,C}=16.4$ mA cm^{-2}, respectively. The corresponding currents according to the measured EQE are $j^{sun}_{EQE,A}=5.4$ mA cm^{-2}, $j^{sun}_{EQE,B}=8.9$ mA cm^{-2}, and $j^{sun}_{EQE,C}=9.7$ mA cm^{-2}, respectively. This means that in device A only 35% of the absorbed photons are converted into current while it is 57% and 59% for device B and C, respectively. A more detailed view of the losses shall be given for device B (and C). In these devices the current according to absorption in active layers is $j^{max}_{active,B}=11.5$ mA cm^{-2} (C: $j^{max}_{active,C}=12.6$ mA cm^{-2}). This means that a photon flux equivalent to 4.1 mA cm^{-2} (C: 3.8 mA cm^{-2}) is lost due to parasitic absorption. Therefore, only 74% (C: 77%) of the photons in device B (C) are absorbed in active layers, where they are converted with an overall IQE^{act} of 77% (C: 77%).

In summary, it is shown that substrate heating during the deposition of the mixed active layer largely improves j_{sc} as well as FF. This is attributed to a stronger phase separation of donor (DCV6T) and acceptor (C_{60}) phase, which increases the IQE reaching values about 70%. The overall IQE, averaged over the whole spectrum, increases from 35% (device A) to 57% (device B). Finally, high PCEs of 4.9 ± 0.2% are achieved for the heated devices B and C. By optical modeling of the absorption in these devices we identify that major losses in quantum efficiency are due to photon absorption in inactive layers, i.e., transport layers and metal electrodes, and that the IQE^{act} of the mixed layer itself reaches values of 83%.

We thank Dr. Selina Olthof for her support and the Europäische Fonds für regionale Entwicklung (EFRE) and the Freistaat Sachsen (Project No. 12717/2112) for funding.

[1] J. Y. Kim, K. Lee, N. E. Coates, D. Moses, T. Q. Nguyen, M. Dante, and A. J. Heeger, Science **317**, 222 (2007).
[2] S. H. Park, A. Roy, S. Beaupre, S. Cho, N. Coates, J. S. Moon, D. Moses, M. Leclerc, K. Lee, and A. J. Heeger, Nat. Photonics **3**, 297 (2009).
[3] P. K. Watkins, A. B. Walker, and G. L. B. Verschoor, Nano Lett. **5**, 1814 (2005).
[4] S. E. Shaheen, C. J. Brabec, N. S. Sariciftci, F. Padinger, T. Fromherz, and J. C. Hummelen, Appl. Phys. Lett. **78**, 841 (2001).
[5] F. Padinger, R. S. Rittberger, and N. S. Sariciftci, Adv. Funct. Mater. **13**, 85 (2003).
[6] G. Li, V. Shrotriya, Y. Yao, J. S. Huang, and Y. Yang, J. Mater. Chem. **17**, 3126 (2007).
[7] K. Suemori, T. Miyata, M. Yokoyama, and M. Hiramoto, Appl. Phys. Lett. **86**, 063509 (2005).
[8] S. Pfuetzner, J. Meiss, A. Petrich, M. Riede, and K. Leo, Appl. Phys. Lett. **94**, 253303 (2009).
[9] D. Wynands, M. Levichkova, M. Riede, M. Pfeiffer, P. Baeuerle, R. Rentenberger, P. Denner, and K. Leo, J. Appl. Phys. **107**, 014517 (2010).
[10] K. Walzer, B. Maennig, M. Pfeiffer, and K. Leo, Chem. Rev. (Washington, D.C.) **107**, 1233 (2007).
[11] E. Centurioni, Appl. Opt. **44**, 7532 (2005).
[12] See supplementary material at http://dx.doi.org/10.1063/1.3475766 for additional verification of the PCE in an outdoor measurement and an additional device with $x_E=20$ nm showing the same behavior of the IQE spectrum.

Increase of internal quantum efficiency in small molecular oligothiophene:C_{60} mixed heterojunction solar cells by substrate heating – Supplemental Material

D. Wynands,* M. Levichkova, K. Leo, and M. Riede

Institut für Angewandte Photophysik, Technische Universität Dresden, 01062 Dresden, Germany

C. Uhrich, G. Schwartz, D. Hildebrandt, and M. Pfeiffer

Heliatek GmbH, 01139 Dresden, Germany

(Dated: August 18, 2010)

I. ADDITIONAL DEVICES

In addition to the devices presented in the paper we investigated two additional devices (D and E) with a mixed layer thickness of x_D=x_E=20 nm. The structure is the same as of devices

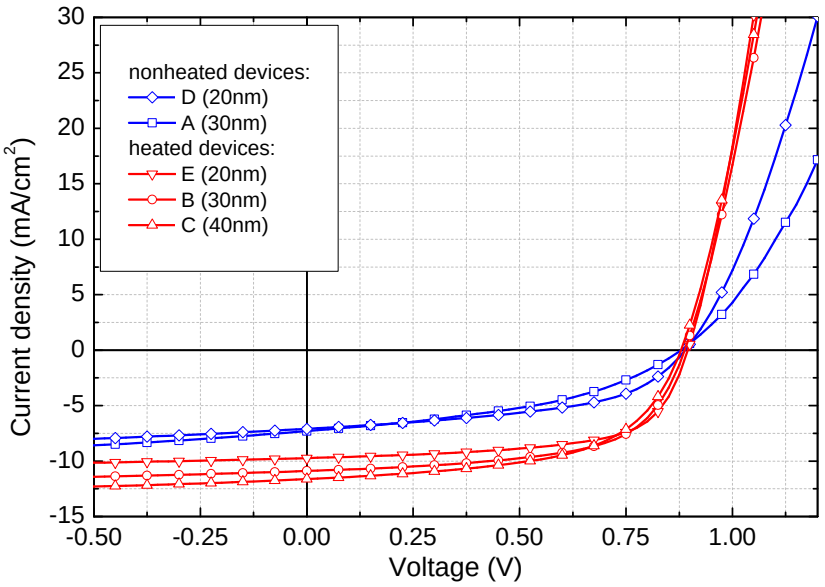

FIG. 1: Current-voltage characteristics of devices A to E. For performance parameters see Table I.

*Electronic address: david.wynands@iapp.de; URL: http://www.iapp.de

TABLE I: Performance parameters of devices A to E.

device	V_{oc} (V)	j_{sc} (mAcm^{-2})	FF	I (mWcm^{-2})	η_{PCE} (%)
A	0.88	7.3	0.422	126.0	2.1±0.1
B	0.89	10.9	0.607	119.3	4.9±0.2
C	0.88	11.6	0.570	117.7	4.9±0.2
D	0.89	7.1	0.503	128.2	2.5±0.1
E	0.90	9.7	0.640	125.9	4.4±0.2

A to C: ITO / n-C_{60} (5)/ C_{60} (15)/ DCV6T:C_{60} (x, T_{sub})/ BPAPF (5)/ p-BPAPF (10)/ p-Di-NPD (30)/ NDP9 (1)/ Al (100). Device D was produced without substrate heating (T_{sub}=30 °C), whereas device E was heated to a substrate temperature of approximately 90 °C during the deposition of the mixed layer. Mixing ratio of the DCV6T:C_{60} HJ is 2:1 by volume. Mixed layer thickness of devices A to E is x_A=30 nm, x_B=30 nm, x_C=40 nm, x_D=20 nm, x_E=20 nm, respectively.

Fig. 1 presents the current-voltage characteristics of all investigated devices. Performance parameters are summarized in Table I. Due to to the smaller mixed layer thickness of the additional devices D and E they exhibit smaller short circuit currents (D: 7.1 mAcm^{-2}, E: 9.7 mAcm^{-2}) than corresponding devices, but are characterized by a slightly higher fill factor (D: 0.503, E: 0.640). The enhanced power conversion efficiency (PCE) of device E compared to device D underlines the positive effect of substrate heating.

In Fig. 2 IQE spectra of the heated devices B, C, and E are shown. As stated in the paper all devices exhibit nearly equal IQE despite their difference in mixed layer thickness. This shows that η_{cc} has no observable limiting effect on the IQE upon the investigated interval. We therefore assume that the mixed layer morphology achieved by substrate heating is considerably optimized.

II. ADDITIONAL CHECK OF POWER CONVERSION EFFICIENCY

To confirm the determined PCE of device B and C we conducted outdoor measurements on the balcony of our institute (51 ° 3'N, 13 ° 44' 24"E) on 09.08.2009. An aperture of 2.985 mm^2 was used. Intensity of sun irradiation was 99 mWcm^{-2} determined by an outdoor

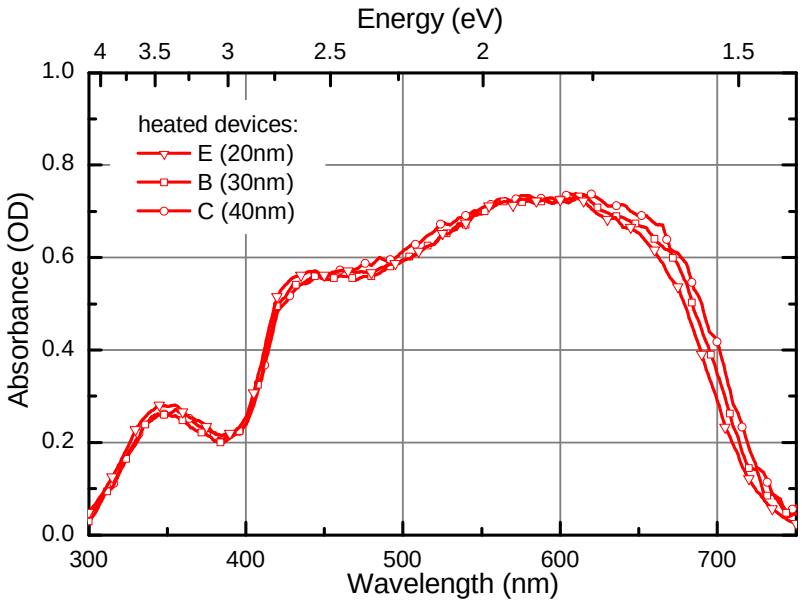

FIG. 2: Internal quantum efficiency of devices B, C and E.

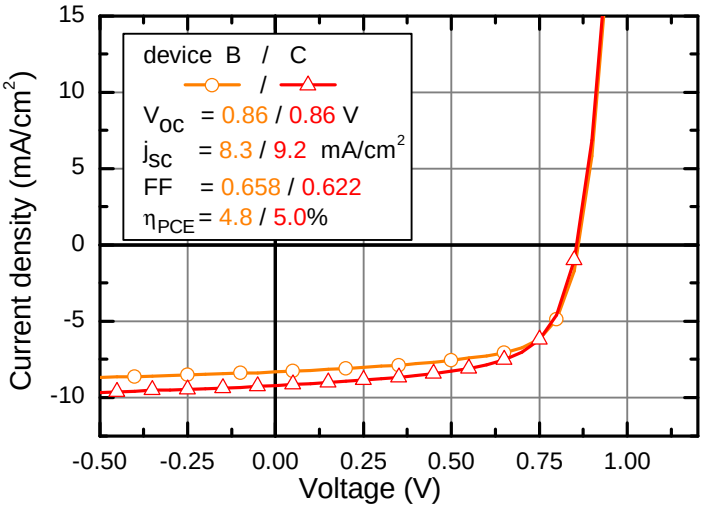

FIG. 3: Current-voltage characteristics of devices B and C in outdoor measurement. Perfomance parameters are given in the inset. Intensity is determined by an outdoor reference cell.

reference cell (Fraunhofer Institute for Solar Energy Systems, Freiburg, Germany). In Fig. 3 the corresponding current-voltage curves are presented. Temperature of the assembly platform was 32.8 °C. Nevertheless, a higher temperature of the devices during the measurement has to be expected. We estimate the device temperature to be around 45 °C since the device could not be cooled directly. By this reason a higher fill factor and a lower open circuit

voltage are observed as compared to the reported measurements under sun simulator. However, PCEs of 4.8 % and 5.0 % are determined for device B and C, respectively. Thus, the reported efficiencies for these devices are confirmed.

III. OPTICAL MODEL

To separate the absorption of active absorber layers from absorption within transport layers and metal contact, we use a transfer-matrix-formalism to model the device optically [1]. Values of the optical constants n and k were derived by fitting transmission and reflection spectra of thin film layers of the respective materials [2]. However, the accuracy of these values is limited, in that they do not account for the effect of dopant admixture into Di-NPD and C_{60}. Optical constants of BPAPF were measured with dopant, although a thin neat layer of BPAPF is also used in the device. The mixed layer optical constants were determined on a heated quartz glas substrate. That means, we can not account for the influence of the C_{60} underlayer or a possible spatially-dependence of the mixed layer optical constants with this method. In Fig. 4 the calculated absorption profile of devices B, C, and D are presented to show that the thinfilm optics of device B and C is optimized for maximum absorption in the mixed active layers.

IV. REFERENCES

[1] E. Centurioni. *Applied Optics*, 44(35):7532–7539, 2005.

[2] T. Fritz, J. Hahn, and H. Boettcher. *Thin Solid Films*, 170(2):249–257, 1989.

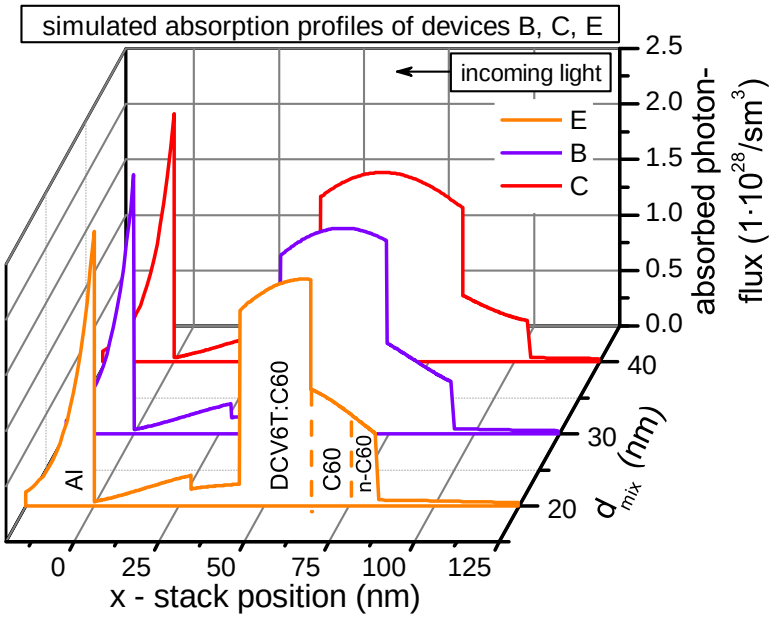

FIG. 4: Absorbed photon flux within device B, C and E as calculated by optical modelling. In device B and C, the absorption profile exhibits a maximum in the mixed layer showing that the choosen transport layer thickness is optimal for maximized absorption. In device E the maximum is not reached, meaning that a slightly higher hole transport layer thickness would be needed for optimized absorption.